ACS APPLIED OPTICAL MATERIALS

pubs.acs.org/acsaom Article

Switchable Bragg Reflections via Controllable Inner Particle Motion in Yolk−Shell Colloidal Crystals

Hikaru Namigata, Tom A. J. Welling, Kanako Watanabe,* Keishi Suga, Arnout Imhof, Alfons van Blaaderen, and Daisuke Nagao*

Cite This: *ACS Appl. Opt. Mater.* 2024, 2, 181−190 Read Online

ACCESS | Metrics & More | Article Recommendations | Supporting Information

ABSTRACT: Yolk−shell particles consist of a hollow shell enclosing a mobile inner particle. Colloidal crystals made from yolk−shell particles are a unique structure, in which the disorder of highly scattering inner particles can be controlled, which allows for optical switching. In this work, yolk−shell particles were synthesized and assembled into an ordered structure. External alternating current (AC) electric fields were used to control the inner particle motion, as observed by confocal microscopy and optical reflection measurements. The colloidal crystal of yolk−shell particles showed long-range order due to the assembled shells but decreased short-range order due to the Brownian motion of inner particles. Using an AC electric field (25 V/mm), all inner particles moved electrophoretically, resulting in ordered inner-particle arrangements. This enabled the fast, reversible switching of the Bragg reflection intensities. Next, we investigated how a decreased short-range order when the field is off influenced the switchability. The largest optical intensity change was achieved with a high ionic strength (10 mM) and a small core-to-shell size ratio (∼0.3). Our proof-of-concept results show promise that with further optimization, even more strongly switchable photonic crystals can be achieved in this way.

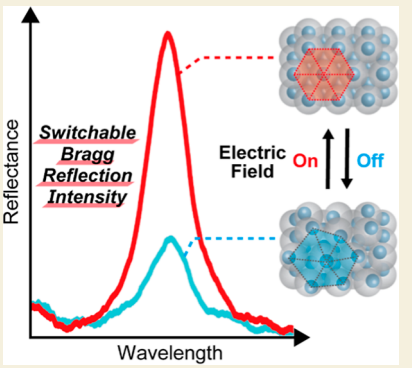

KEYWORDS: *yolk−shell particles, colloidal crystals, alternating current electric fields, electrostatic interactions Debye−Waller factor*

1. INTRODUCTION

States of matter such as solid, liquid, and gas are classified depending on the range at which the components, i.e., atoms and molecules forming the state are ordered. Materials for which building blocks are arranged with both long-range order in position and orientation are known as crystals. A dense solid state without long-ranged positional order is called an amorphous or glassy state, while fluids additionally have mobility of the atoms and molecules that are lacking for solids, or extremely slow on experimental time scales. Analogous to the atomic scale, dispersions of colloidal particles also can form these different phases. The solid assemblies of nano- to micron-sized colloidal particles with long-range order are commonly called colloidal crystals[1−5] and those with short-ranged order are called colloidal glasses.[6−8]

Colloidal crystals consisting of submicrometer-sized particles reflect specific (visible) light wavelengths according to Bragg's law, analogous to atomic or molecular crystals exhibiting specific X-ray diffraction patterns. As such, colloidal crystals with interparticle spacings on the length scales of visible wavelengths of light are also referred to as photonic crystals, and they have been studied for various applications in optics such as color pigments,[9−11] anticounterfeiting labels,[12,13] and colorimetric sensors.[14,15] Bottom-up fabrication methods for three-dimensional (3D), multilayered, colloidal crystals have been studied extensively. Self-assembled crystals can be fabricated on a large (∼cm^2) scale,[16,17] and the number of layers is easily controlled.[18−20] However, in general, the rearrangement of building blocks in close-packed crystals is barely possible because the building blocks do not have any free space to move. This results in static optical properties, meaning that the Bragg reflection wavelengths and intensities cannot easily be tuned. Colloidal crystals of which the Bragg reflection can be dynamically controlled, so-called switchable colloidal crystals[21−23] have increased potential for applications such as displays[7,24] or e-ink.[25,26]

One possibility to obtain switchable colloidal crystals is to tune the interparticle spacing in the crystals. Bragg peak shifts can then be reversibly controlled by employing, for example, humidity-,[27,28] pH-,[29] or thermo-responsive[30,31] polymer matrices within the interstices of the crystals or by using such polymers as part of the colloidal particles themselves. The interparticle spacing of building blocks that are responsive to external stimuli such as magnetic[32,33] and electric fields[34,35] can be tuned as well if the crystals are not closely packed.

Received: November 1, 2023
Revised: November 29, 2023
Accepted: December 1, 2023
Published: December 20, 2023

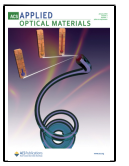

Moreover, reversible control over the crystalline order also allows changing the Bragg reflection intensity, i.e., the degree of constructive interference as opposed to more random, incoherent scattering of light.[36,37] In this approach, however, the transition between disordered and crystalline states has generally been focused on. Such transitions generally have larger response times to achieve the desired effect because of strong hydrodynamic and/or direct interactions between the concentrated particles.

Yolk−shell (or rattle-type) particles, which consist of a hollow shell enclosing a mobile core particle, are promising candidates for building blocks of colloidal crystals with a different kind of control over the coherence in the scattering of the colloidal photonic crystal.[38−40] Because the core particles can move freely within their hollow shells (voids) filled with liquid, colloidal crystals composed of yolk−shell particles are expected to possess tuneability in the spatial distribution of cores if the Brownian motion inside the shell can be controlled,[41] for instance via external stimuli. In atomic and molecular crystals, the attenuation of the Bragg peaks due to thermal motion is described by the Debye−Waller factor (DW: after Peter Debye and Ivar Waller). Similarly, the coherent scattering, or diffraction, of the movable cores inside yolk−shell particles can be significantly reduced even if the shells form a perfectly long-ranged lattice. However, the approach to the melting point limits thermal displacements in molecular crystals, no such limitation exists in yolk−shell colloidal crystals. Therefore, the reduction in coherent scattering can be made much more severe than that would be possible for molecules. Previous reports[42−44] also predicted that the stopbands or photonic band gaps are tuneable when the internal structure of yolk−shell colloidal crystals can be controlled. Our research groups previously demonstrated control over the motion of submicrometer-sized cores within hollow silica shells by applying an external alternating current (AC) electric field. This work showed that the internal arrangement of cores in yolk−shell colloidal crystals is controllable by an external electric field[45,46] and/or the ionic strength.[47] Thus, colloidal crystals of yolk−shell particles are envisioned as a new type of fast, electrically switchable photonic crystal. Switching the coherent scattering through control over the motion of the core particles within the shells can be used to switch the intensities of the Bragg peaks.

In this work, we create 3D yolk−shell colloidal photonic crystals and demonstrate that the Bragg reflection intensities are strengthened and weakened by switching an external AC electric field on/off. In addition, we show that the magnitude of switching can be increased by giving the cores more freedom of movement, either by reducing the electric double-layer thickness and/or increasing the core-to-shell size ratio. We conclude that the reversible control of the optical properties is made possible by control of the displacement disorder (i.e., the randomness of the core arrangement) or the DW factors of the strongly scattering cores of the yolk−shell colloidal photonic crystals with an external electric field.

2. METHODS

2.1. Materials

Tetraethyl orthosilicate (TEOS, 95%), titanium tetraisopropoxide (95%), methylamine aqueous solution (40 wt %), aqueous ammonia solution (NH_3 aq, 25 wt %), acetonitrile (99.5%), ethanol (99.5%), sodium chloride (NaCl, 99.5%), polyvinylpyrrolidone (PVP, weight-average molecular weight M_w = 360,000), styrene (St, 99%), *p*-styrenesulfonic acid sodium salt (NaSS, 80%), potassium persulfate (KPS, 95%), lithium chloride (LiCl, 99%), and dimethyl sulfoxide (DMSO, 99%) were purchased from FUJIFILM Wako Pure Chemical Corporation (Osaka, Japan). The inhibitor for the St monomer (*p*-*t*-butylcatechol) was removed by an inhibitor removal column. Poly(allylamine hydrochloride) (M_w = 50,000) was obtained from Sigma-Aldrich Japan (Tokyo, Japan). The silane coupling agents 3-methacryloxypropyltrimethoxysilane (95%) and 3-aminopropyltriethoxysilane (APTES, 98%) were purchased from Shin-Etsu Chemical (Tokyo, Japan). Ultrapure water was produced by a water purification system (Direct-Q 3UV, Merck).

2.2. Synthesis of Silica@titania@silica (S/T/S) Core Particles

S/T/S particles were prepared via hydrolysis−condensation of metal alkoxide monomers in water ethanol mixtures through basic ammonia-induced catalysis. The detailed synthesis procedure is described in Supporting Information (Figure S1). Briefly, a titania-coating on silica particles (silica@titania) was performed by following our previous report.[3] The silica@titania particles were coated with an extra silica layer.[48,49] The TEM images of silica, silica@titania (S/T), and S/T/S are shown in Figures S2a and S3a−c.

2.3. Synthesis of Yolk−Shell Particles Incorporating a S/T/S Core

The yolk−shell particles which consist of a S/T/S core and a hollow, porous silica shell were prepared by following steps:[45,50,51] (1) the core particles were coated with a polystyrene (PSt) layer as a sacrificial layer, (2) a silica coating process was conducted on the PSt-coated particles, and (3) the PSt layers were removed by calcination (500 °C in air for 4 h). The details of each procedure and synthesized particles are presented in the Supporting Information. The heat treatment also promotes the crystallization of TiO_2 from the amorphous to anatase phase,[50] which increases the refractive index. Because the core particles were stuck on the inner wall of silica shells after the heat treatment, the inner silica shell walls were dissolved slightly in NH_3 aq (pH ∼11). After 15 min of sonication, the particle suspension was stirred for 1.5 h at 40 °C. The particles were centrifuged more than four times and redispersed in water. As mentioned in the Supporting Information, APTES was also used as a silica precursor for the formation of the inner shell of silica. The APTES-containing silica shells have a less-condensed silica framework compared to that of outer silica shells which was prepared with only TEOS, resulting in the preferential dissolution of the silica inside the outer shell walls.

2.4. Fabrication of 3D Yolk−Shell Colloidal Crystals

The yolk−shell particles were dispersed in 0.2 mM LiCl aqueous solution and injected into a quartz cell (1.0 × 10 × 45 mm, AS ONE, Q-101). The cell was fixed perpendicular to the ground for 1 week to settle the particles gravitationally. After the colloidal crystal was formed, concentrated LiCl aq was added to adjust the LiCl concentration to 2.0 or 10 mM. The colloidal crystals were left for more than 2 weeks to ensure that they reached equilibrium. To apply an external AC electric field to the colloidal crystals, two copper wires (KYOWA HARMONET, ⌀ = 0.8 mm) with the polyurethane coating removed were inserted on both sides of the colloidal crystal (Figure S4).

2.5. Characterization

The prepared particles and assemblies were observed using a field-emission scanning transmission electron microscope (FE-STEM, Hitachi, HD-2700) and a field-emission scanning electron microscope (FE-SEM, Hitachi, S-4800), respectively. The volume−averaged diameter was determined by measuring more than 200 particles in the TEM images. The zeta potential of the synthesized particles was measured with a zeta-potential analyzer (Otsuka Electronics, ELSZ-2). The Smoluchowski equation was used to relate the electrophoretic mobility to the zeta potential. The reflection spectra were measured by a fiber multichannel spectrometer (SOMA OPTICS, model S-2630) equipped with a halogen lamp (SOMA OPTICS, S-2650). One reflection spectrum was obtained by accumulating 10 acquisitions

https://doi.org/10.1021/acsaom.3c00392
ACS Appl. Opt. Mater. 2024, 2, 181−190

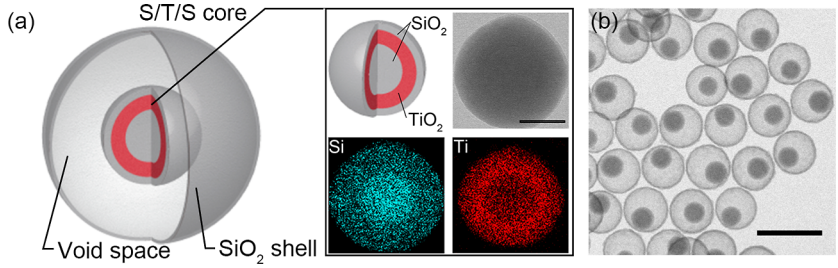

Figure 1. (a) Schematic illustration of a yolk−shell particle and a TEM image of a S/T/S core particle and the corresponding STEM−EDX intensity mapping images. The scale bar is 150 nm. (b) TEM image of yolk−shell particles composed of a SiO_2@TiO_2@SiO_2 (S/T/S) core particle and a silica shell. The outer shell diameter, core diameter, and shell thickness were d_V = 690 nm (C_V = 3.1%), d_{core} = 330 nm (C_V = 5.7%), and t_{shell} = 30 nm, respectively. The scale bar represents 1 μm.

with an exposure time of 15 ms. For each condition, the reflection spectra measurement was repeated at least three times with short intervals. In the measurement, a quartz cell filled with water was used as a reference cell. An external AC electric field was applied with a function generator (GWINTEK, SFG-2004) and an amplifier (NF Circuit Design Bloc, HSA4011). The peak-to-peak field strength (V_{pp}) was measured with a digital oscilloscope (GWINTEK, GDS-1062A). Because the raw reflection spectra were noisy and contained a background, the baseline was estimated and removed via the asymmetric least squares method.[52,53] The baseline-removed spectra were subsequently smoothed with a Savitzky−Golay filter.

The observation of core motion in a 2D array with/without an external AC electric field was carried out using a confocal microscope (Leica, TCS SP8) in the reflection mode with a super continuum white light laser (NKT Photonics, SuperK). The frame rate was 25 fps. The dispersion of yolk−shell particles was dropped onto a cover glass, which had been glow-discharged (Cressington 208) for 10 s at 5 mA. The dispersion was left until the solvent (deionized water) had almost evaporated. When a 2D array of yolk−shell particles was formed, a solution of 85/15 (v/v) DMSO/water (refractive index n = 1.46 at 25 °C, λ = 546 nm[54]) with 2.0 mM LiCl was added to index-match the silica.[55]

For the tracking of core particles within a shell, the motion of a single core particle was captured by the confocal microscope with a frame rate of 45 fps (3000 frames in total). The frames consisted of 64 × 64 pixels (41.34 nm/pixel). The confocal microscopy images were converted to TIFF images by using Fiji ImageJ software. The images were analyzed by using Trackpy (v0.4.2) to acquire the trajectories of the core motion.

3. RESULTS AND DISCUSSION

3.1. Ordering of the Arrangement of Core Particles in a Yolk−Shell Colloidal Crystal with an External AC Electric Field

Figure 1a,b shows a schematic illustration and a TEM image of the yolk−shell particles prepared as the building blocks of the photonic crystals. Highly monodisperse yolk−shell particles consisting of a core (volume averaged diameter d_V = 330 nm, coefficient of variation C_V = 5.7%) and a hollow silica shell (d_V = 690 nm, C_V = 3.1%) were synthesized. Equations S1 and S2 are used to calculate d_V and C_V of the synthesized particles. Energy-dispersive X-ray (EDX) spectroscopy mapping (the inset of Figure 1a) indicates that the movable inner particle was composed of silica and titania shells with an innermost silica particle and the titania layer in the middle (SiO_2@TiO_2@SiO_2, S/T/S). For building blocks of colloidal photonic crystals, monodisperse particles with a high refractive index are often desirable. In this paper, we designed S/T/S particles as the cores to achieve the above requirements since monodisperse silica spheres are easier to achieve than monodisperse titania particles. We chose to grow titania shells onto monodisperse silica cores (d_V = 180 nm, C_V = 4.7%) as the bases for the scattering cores;[17,56−59] titania is well-known as a high refractive index material.[8,60] Hollow porous silica particles were employed as the shell of the yolk−shell particles in order to limit the light scattering of the shells as compared with that of the cores. For example, the scattering strength of the S/T/S core in water was more than 20 times higher than that of the hollow shell in the range of wavelengths λ = 400−1000 nm (Figure S5). Detailed procedures of the yolk−shell particle synthesis and characterization can be found in the Methods Section and Supporting Information (Figures S1−S3).

To directly observe the core motion within their shells and the differences in the core particles' displacement with/without an external AC electric field, an ordered 2D array of yolk−shell particles was fabricated by drop-casting the particle dispersion onto a precleaned glass slide. Immediately after most of the original solvent (deionized water) had evaporated, an aqueous DMSO solution [DMSO/water = 85/15 (v/v)] with 2.0 mM LiCl was dropped onto the 2D colloidal array. Since the DMSO/water mixture has almost the same refractive index as silica (1.46 at 25 °C, λ = 546 nm),[54,55] the silica shells were hardly visible in reflected light confocal microscopy, and only the cores were observed. We tried to observe the core motion at 100 Hz, which was the same frequency as that used in optical measurements shown in the next section, but it was hard to follow the core motions (frame rate: 45 fps; Movie S1). Therefore, an external AC electric field with a lower frequency (E = 25 V/mm, f = 1 Hz) was applied to the 2D array so that the core motion could be easily observed with the confocal microscope (Movie S2, frame rate: 25 fps). When the field is off, the cores are seen to undergo random Brownian excursions around their lattice positions. However, as soon as the field is turned on, the cores begin to oscillate in unison at the frequency of the electric field.

Figure 2a,b shows stills of Movie S2, the core motion with/without applying the electric field, where the green signals are caused by the reflected and scattered light from the core particles. Figure 2a presents stills of Movie S2 when the field was off. The core particles exhibited random Brownian motion within the shells, which led to a distorted hexagonal arrangement of cores, as illustrated by the blue dashed lines. On the other hand, Figure 2b presents stills when the electric field was applied (25 V/mm, 1 Hz). The core motion changed from random to parallel and in lockstep with the electric field, which meant that the cores remained in a well-ordered hexagonal structure throughout their oscillation. This parallel motion is due to particle electrophoresis within the shells.[46] The difference in the core arrangement with the electric field

https://doi.org/10.1021/acsaom.3c00392
ACS Appl. Opt. Mater. 2024, 2, 181−190

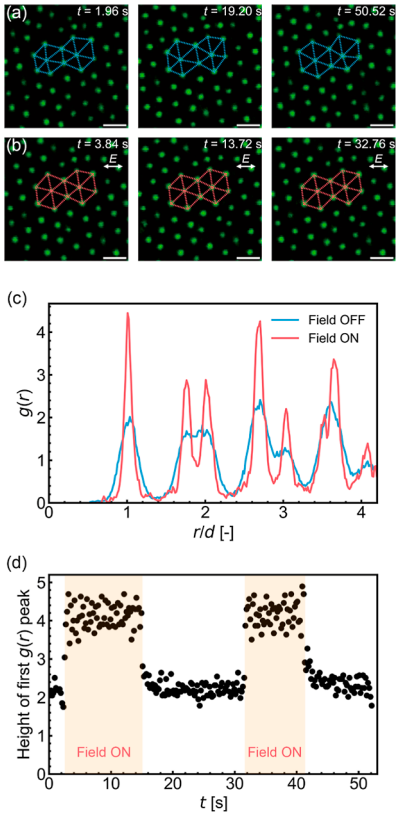

Figure 2. (a,b) Confocal microscopy images of the core particles in a 2D array of yolk−shell particles in 85/15 v % DMSO/water with 2.0 mM LiCl. (a) Stills of Movie S2 without AC electric fields, and (b) those with an AC electric field on. Electric field intensity E = 25 V/mm, and the frequency f = 1.0 Hz. The scale bars represent 1.0 μm. (c) Radial distribution function $g(r)$ averaged over frames with the AC electric field either on or off. $g(r)$ is plotted against the distance from each reference particle, which is normalized by the outer shell diameter (r/d). (d) Time evolution of the height of the first peak in the radial distribution function $g(r)$ (at $r/d \approx 1$).

on or off was evaluated by the 2D radial distribution function $g(r)$. Figure 2c presents $g(r)$ plotted against the distance (r) divided by the outer shell diameter (d). Peak positions in the plots showed that the cores were arranged hexagonally both with and without the electric field due to the shells being assembled in a hexagonal structure. However, because of the well-ordered arrangement of cores with the field on, sharper peaks were observed compared to the case with the field off. Figure 2d shows the time evolution of the first peak of $g(r)$ when the electric field is applied to the 2D array multiple times.

The height of the first peak was reversibly increased/decreased shortly after switching the electric field on/off, which implies that the change in motion occurred immediately after applying the electric field.

3.2. Switchable Bragg Reflection Intensity from Yolk−Shell Colloidal Photonic Crystals

As mentioned in Section 3.1, the coefficient of variation, or polydispersity, of the yolk−shell particles was low enough to self-assemble into well-ordered colloidal crystals.[61−63] A three-dimensionally ordered colloidal crystal of yolk−shell particles was fabricated on a silicon substrate by a drop-casting method (Figure S6a). The obtained dried colloidal crystal exhibited angle-dependent reflection peaks, which correspond to the theoretical values estimated according to Bragg's law (Figure S6b,c). Because the cores got stuck on the inner shell wall by drying, gravitational sedimentation[64−67] was performed as an alternative way to create yolk−shell colloidal crystals in liquid with mobile cores inside. The synthesized yolk−shell particles were dispersed in an aqueous LiCl solution [LiCl concentration (C_{LiCl}) = 2.0 mM]. The particles sedimented to the bottom of a quartz cell in 1 week, forming an ordered colloidal crystal.

When an external AC electric field is applied (field strength E = 24 V_{pp}/mm and frequency f = 100 Hz), the intensity of the reflection peaks at wavelengths λ = 846 and 565 nm increased without shifting the peak wavelength or affecting the peak width at half-maximum (Figure 3a). These peaks can be

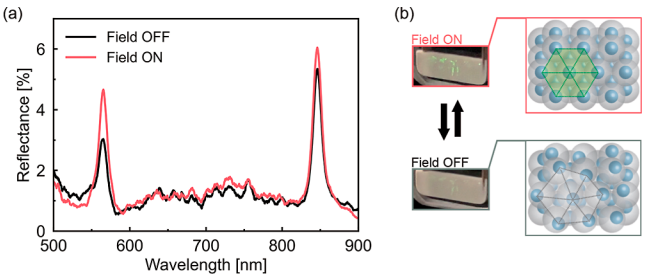

Figure 3. (a) Reflection spectra of the yolk−shell colloidal crystal in an aqueous LiCl solution (C_{LiCl} = 2.0 mM) measured with or without applying an AC electric field. Electric field intensity E = 24 V_{pp}/mm, and the frequency f = 100 Hz. (b) Photographs of the yolk−shell colloidal crystal with an AC electric field on (top) or off (bottom) and corresponding schematics of core particle arrangement in the yolk−shell colloidal crystal.

assigned to the (222) and (333) planes of the face-centered cubic (fcc) structure, respectively (detailed peak assignment is described in the Supporting Information). The nearest neighbor particle distance was estimated from Bragg's law to be approximately 740 nm, which was 50 nm longer than the outer shell diameter (690 nm). This is because of electrostatic repulsion between the negatively charged outer shells; in a 2.0 mM LiCl solution, the outer shells of yolk−shell particles have 6.8 nm of the Debye length κ^{-1}, and the surface distance is expected to be 40−45 nm when considering electrostatic repulsion and van der Waals attraction between the particles (Figure S7). The detailed equations are presented in Supporting Information (eqs S6−S9). The sum of the outer shell diameter and the surface distance was in good agreement with the nearest neighbor distance estimated from the reflection spectra.

The ratios of the peak intensities observed with and without the electric field (I_{on}/I_{off}) were approximately 1.1 and 1.5 for the (222) and (333) planes, respectively. The structural color corresponding to the reflection peak of the (333) plane (λ = 565 nm) was clearly confirmed by the naked eye when the field had been turned on and the intensity of the green reflection increased (Figure 3b and Movie S3). This switching of the Bragg peak intensities was reversible and took less than 0.3 s, which was the maximum shutter speed of the spectrophotometer. Such reversible switching was caused by the electric-field-induced change in core motion within the shell. Because the inner core particles were mobile within the hollow silica shells even though the hollow shells were densely packed, only the cores were expected to respond to the applied electric field,

https://doi.org/10.1021/acsaom.3c00392
ACS Appl. Opt. Mater. 2024, 2, 181−190

as we previously observed by analyzing single yolk−shell particles (see, e.g., refs 45−47). Therefore, as expected, a colloidal crystal from hollow silica particles without the core particles did not change its reflection peak intensity in response to similar electric fields (Figure S8).

The influence of the field frequency on the switchability of the Bragg reflection intensity was also investigated. External electric fields with various frequencies (f = 50−1000 Hz, E = 24 V_{pp}/mm) were applied to the 3D yolk−shell colloidal crystal, and Bragg peak intensity ratios with/without fields were calculated (Figure 4). At frequencies lower than 400 Hz,

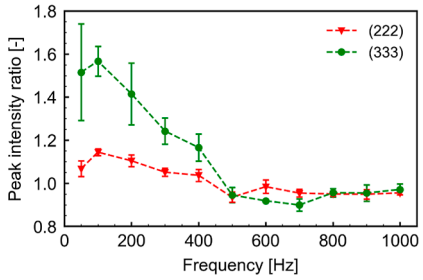

Figure 4. Reflection peak intensities of a yolk−shell colloidal crystal in LiCl aq (C_{LiCl} = 2.0 mM) with AC electric field application of different frequencies (E = 24 V_{pp}/mm, f = 50−1000 Hz).

reflection peaks were strengthened by applying electric fields; however, the ratio gradually decreased with an increase in the frequency. The peak intensities were scarcely increased with electric fields at $f \geq 500$ Hz. This is likely because at high frequencies, the cores were unable to follow the electric field by moving from one side of the shell to the other, as was observed before in measurements on single particles,[46] resulting in almost no change in the arrangement of cores. It is expected that the frequency at which the switchability can be performed is increased at higher electric field strengths due to faster electrophoresis of the core particles.

3.3. Effect of the Electrolyte Concentration on the Peak Intensity Switchability

The difference in the reflection peak intensities measured with and without an electric field is an indicator of the effectiveness of the switchability of yolk−shell colloidal crystals. We have shown that it results from the cores making random displacements versus taking on near-perfect relative positions. A larger switching ratio could be obtained by expanding the motion range of the core particles. One way to do this is to reduce the range of electrostatic repulsion between the core and the shell, which are both negatively charged. This range can be reduced by decreasing the Debye length κ^{-1} (i.e., thickness of the electric double layer) by increasing the electrolyte concentration in the surrounding medium. In this section, we raise the electrolyte concentration to C_{LiCl} = 10 mM (corresponding κ^{-1} was 3.0 nm). From our previous report, cores can get significantly closer to the inner shell walls by increasing the electrolyte concentration.[47] The reflection spectra of a yolk−shell colloidal crystal in a 10 mM LiCl solution when the electric field was turned on and off are shown in Figure 5a. The reflection peaks attributed to the (222) and (333) planes were again observed, but this time the reduction in height is clearly larger than that in the case of the colloidal crystal in a 2.0 mM LiCl solution. Figure 5b displays the calculated reflection peak ratios when the field is on/off

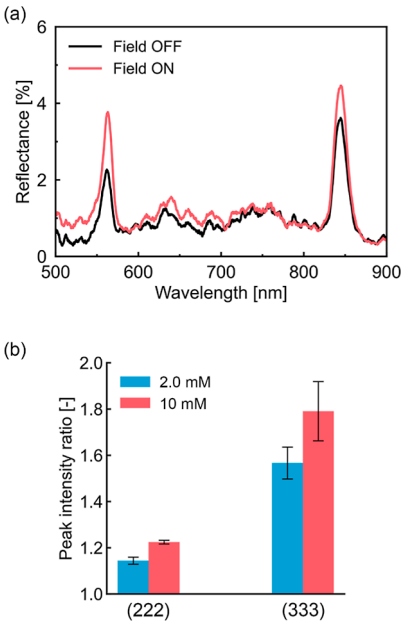

Figure 5. (a) Reflection spectra of a yolk−shell colloidal crystal in LiCl aq (C_{LiCl} = 10 mM) measured with or without applying an AC electric field (E = 24 V_{pp}/mm, f = 100 Hz). The Bragg reflection peak wavelengths are 563 and 845 nm. (b) Intensity ratios of the reflection peaks obtained with applying an AC electric field to that obtained without a field (C_{LiCl} were 2.0 and 10 mM where κ^{-1} were 6.8 and 3.0 nm, respectively).

(described as I_{on}/I_{off}) where C_{LiCl} = 2.0 or 10 mM. For both (222) and (333) planes, I_{on}/I_{off} values were larger for the colloidal crystal in 10 mM LiCl compared to those in 2.0 mM LiCl, which shows that the switchability can be enhanced by adding electrolytes. This was because the randomness of the core arrangement increased when the motion range of cores expanded.

3.4. Effect of Core Size on the Peak Intensity Switchability

Another way to expand the relative motion range of core particles is to make the cores smaller compared to the void size. As shown in Figure S3f, we prepared different yolk−shell particles that contained a smaller core (d_{core} = 210 nm, C_V = 9.2%). The diameter and thickness of the hollow porous silica shells were comparable to those of the yolk−shell particles shown in Figure 1. The positions of both the large and small core particles were tracked within their shells in the absence of an electric field using confocal microscopy. Figure 6 shows 2D projection maps of the cores' positions in a certain time range (approximately 1 min). The probability of finding a core at a certain radial distance from the center of its shell is also shown, and the (2D projection of the) mean square distance $\langle u^2 \rangle$ from the center can be calculated from the probability. As shown in Figure 6a, for the larger cores (d_{core} = 330 nm, Figure 1b), the cores' motion range was only slightly expanded by increasing the electrolyte concentration from 2.0 to 10 mM ($\sqrt{\langle u^2 \rangle}$ = 56 and 64 nm for C_{LiCl} = 2.0 and 10 mM, respectively), which explains the small difference in the reflection intensities with/without the electric field in Figure 5. For the smaller cores, on the other hand, a significant difference in the motion range of the cores between 2.0 and 10 mM was observed (Figure 6b, $\sqrt{\langle u^2 \rangle}$ = 73 and 87 nm for C_{LiCl} = 2.0 and 10 mM, respectively). This suggests that making the

https://doi.org/10.1021/acsaom.3c00392
ACS Appl. Opt. Mater. 2024, 2, 181−190

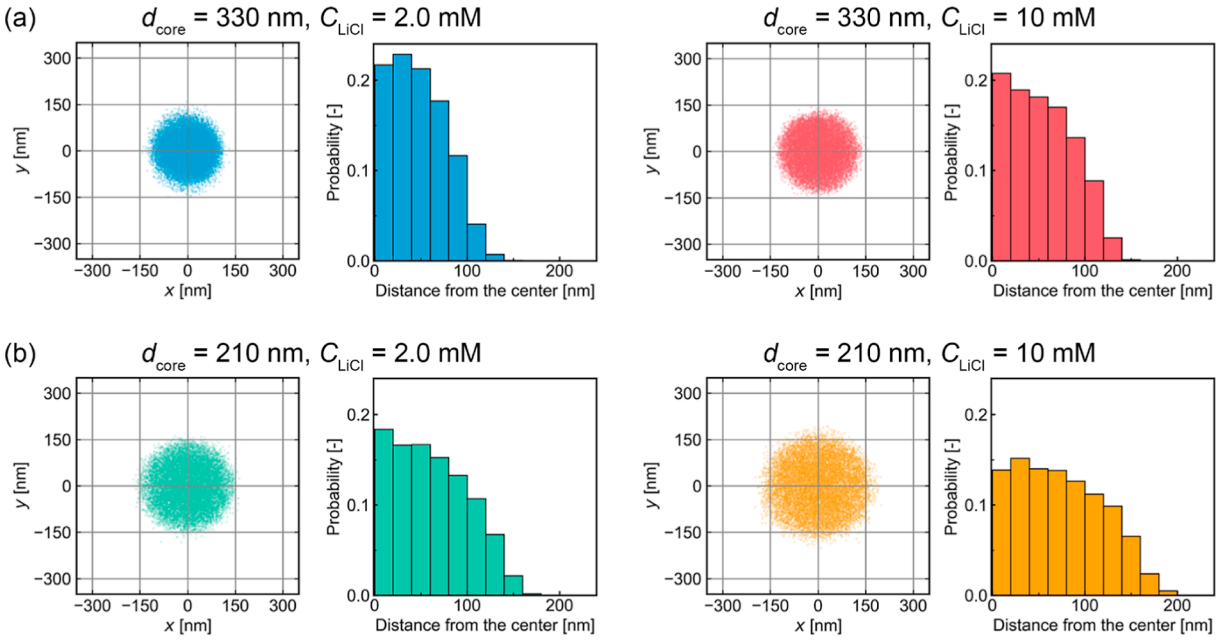

Figure 6. Two-dimensional projection maps of the position of core particles within a shell and the probability of finding the particle a certain radial distance from the center of the shell. (a,b) Results of larger cores (d_{core} = 330 nm) and smaller cores (d_{core} = 210 nm), respectively.

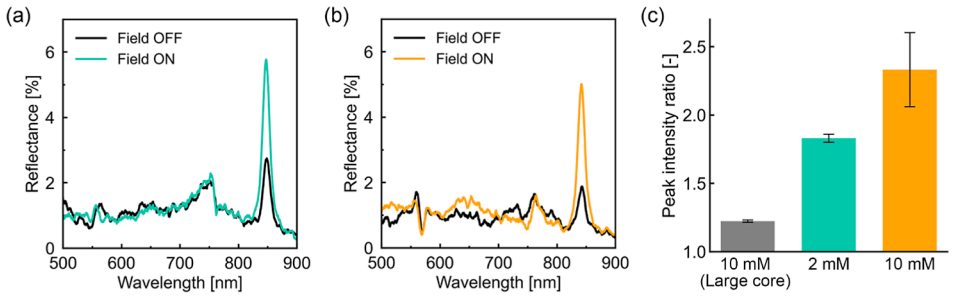

Figure 7. (a,b) Reflection spectra of the yolk−shell colloidal crystals (d_V = 700 nm and d_{core} = 210 nm) in LiCl aq measured with or without applying an AC electric field (E = 24 V_{pp}/mm, f = 100 Hz). C_{LiCl} were (a) 2.0 and (b) 10 mM. The reflection peak wavelengths of (a,b) were 845 and 842 nm, respectively. (c) Ratios of reflection peak intensity obtained with applying an AC electric field to that obtained without a field (C_{LiCl} = 2.0 and 10 mM).

core size smaller is more effective in enlarging the cores' motion range than increasing the electrolyte concentration, at least for the parameter range studied here. Smaller core particles come with the downside of a significantly smaller scattering cross section, as well as the scattering strength of the cores decreases roughly with the square of the volume of the particles (see also Figure S9); however, our recent work has shown that core particle sizes of around 100 nm can still facilitate highly reflective colloidal crystals.[12,68] It should be noted that the motion range of cores was measured in the DMSO/water mixture instead of deionized water. Although the zeta potentials of core particles in DMSO/water were different from those in water, the zeta potentials decreased with increasing the electrolyte concentration as in water (Table S1).

Figure 7a,b displays reflection spectra of yolk−shell colloidal crystals with the smaller cores in two different LiCl solutions (C_{LiCl} = 2.0 and 10 mM). Bragg reflection peaks at λ = 845 and 842 nm were observed from the colloidal crystals in C_{LiCl} = 2.0 and 10 mM, respectively. Those peaks were assigned to the (222) plane; however, the peaks from (333) were not observed in both spectra. This is likely because of the lower scattering intensity for the fcc (333) direction compared to that for (222). As indicated in Figure S10, the (333) reflection coincidentally falls precisely in a minimum of the form factor for the smaller cores. Therefore, the scattering intensity of the (333) peaks decreased below the noise level. As shown in Figure 7a,b, due to the difference in the motion range, a lower peak intensity of the (222) reflection was observed for the colloidal crystal of the smaller cores in a 10 mM LiCl solution compared to that in a 2.0 mM LiCl solution. Most interestingly, the peak intensity ratio I_{on}/I_{off} by electric field switching was greater than 2 for the colloidal crystal with the smaller cores, which was a significant increase compared to that of the colloidal crystal with larger cores in 10 mM (Figure 7c).

The attenuation of reflection peak intensities as a result of the random (thermal) motion of components from their ideal lattice points can be described by the DW factor. Even though the theory was originally developed for atomic/molecular crystals, this also applies to colloidal crystals[69] because it does not rely on the details of the interactions nor on the dynamics of particle motion. For the yolk−shell colloidal crystals, the more ordered core arrangement under the lower frequency

https://doi.org/10.1021/acsaom.3c00392
ACS Appl. Opt. Mater. 2024, 2, 181−190

electric field, which induces collective electrophoretic motions of cores, can be considered as the "ideal" fcc structure with only disorder from the polydispersity of the shells. Therefore, the ratio of Bragg reflection intensity with the electric field on (I_{on}) to that with the electric field off (I_{off}) can be approximated as follows

$$\frac{I_{off}}{I_{on}} = \exp\left[-\frac{2}{3}\pi^2 L^2 (h^2 + k^2 + l^2) \right] \quad (1)$$

$$L = \frac{\langle u^2 \rangle^{1/2}}{r_{nn}} \quad (2)$$

where $<u^2>$ is the averaged squared distance of a particle from its lattice position, r_{nn} is the nearest neighbor distance, and h, k, and l are the Miller indices of the fcc (hkl) plane. L is also known as the Lindemann parameter. As given in Figure 3, the nearest neighbor distance and Miller indices were determined as r_{nn} = 740 nm and (hkl) = (222) or (333).

Table 1 summarizes I_{on}/I_{off} for the peaks from the (222) planes obtained from reflection spectra and those calculated from DW theory in eq 1, where the Lindemann parameters (eq 2) were obtained from the tracking results presented in Figure 6. Here, we assumed that when the field is on the cores are on a perfect lattice (i.e., L = 0). We realize that these tracking results were obtained from 2D projected confocal microscopy data in a different solvent, but they should still give a relatively good approximation for the observed trends. The spectral-based I_{on}/I_{off} trends roughly agree with the ones calculated from the confocal data, which demonstrates that the Bragg reflection intensity changes can be tuned by the average squared distance of the core from its lattice position as predicted by the DW factor. For comparison, according to previous studies,[70−72] the critical value of L when fcc crystals melt is approximately 0.2, although of course in our case the close-packed shells are not expected to melt. For the yolk−shell colloidal crystals in this study, each L was below that threshold; however, L was increased by increasing LiCl concentration and/or making cores smaller, which can result in larger values than that achieved with photonic crystals of the core particles alone without the shells. Especially, the core particle size, that is to say the core-to-shell size ratio, is important for the switchability of these kind of yolk−shell colloidal crystals. In regard to the (222) reflection, we anticipate that almost fully on/off switching will be achieved when $L \geq 0.24$, which correspond to $\sqrt{\langle u^2 \rangle} \geq 180$ nm. Since the yolk−shell particles synthesized in this work had shells with a void diameter around 650 nm, the cores' average displacement of 180 nm is already allowed geometrically. However, to reach the true potential of the approach for the (222) reflection, the Lindemann parameter should be increased by making smaller core sizes. Note that a minimum in the form factor should be avoided, and index matching of silica shells is also desirable.

Table 1. Bragg Peak Intensity Ratios (I_{on}/I_{off}) for the Peaks Attributed to fcc (222) and the Lindemann Parameter L for the Yolk−Shell Colloidal Crystals in LiCl aq (C_{LiCl} = 2.0 or 10 mM)

d_{core} [nm]	C_{LiCl} [mM]	I_{on}/I_{off} (measured)	I_{on}/I_{off} (calculated)[a]	L (measured)
330	2.0	1.14	1.57	0.076
	10	1.22	1.79	0.086
210	2.0	1.83	2.15	0.099
	10	2.33	2.95	0.117

[a]The theoretical I_{on}/I_{off} and L were calculated by considering the particle tracking result shown in Figure 6, which was performed in silica index matching 85/15 (v/v) DMSO/water solution.

Switching the Bragg reflection intensity from colloidal crystals of yolk−shell particles will certainly widen the application possibilities of switchable colloidal crystals such as in color displays, sensors, and optical communication devices with appropriate material design but possibly in switchable colored paint as well.

4. CONCLUSIONS

In summary, a new type of switchable yolk−shell colloidal crystal, in which the internal structure can be reversibly controlled by tuning the displacement of the mobile cores, was

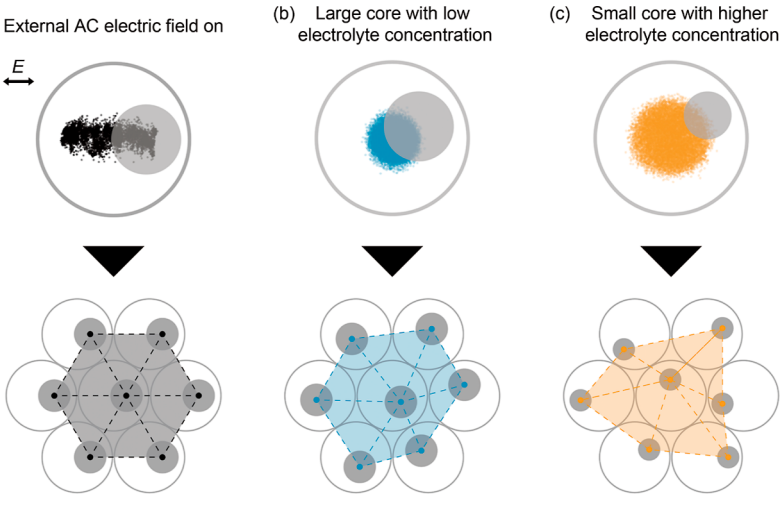

Figure 8. Schematic illustrations of the displacement of the cores and the corresponding arrangements of the core particles in the colloidal crystals: (a) with an external AC electric field on, (b) without external electric fields, a low electrolyte concentration (2.0 mM), and a large core size (d_{core} = 330 nm), and (c) without external electric fields, a high electrolyte concentration (10 mM), and a small core size (d_{core} = 210 nm).

https://doi.org/10.1021/acsaom.3c00392
ACS Appl. Opt. Mater. 2024, 2, 181−190

developed. The intensity of the Bragg reflection peaks of the colloidal crystals was increased/decreased by switching an external AC electric field at a subsecond time scale. The response time of this system is superior to other switching approaches[73,74] and is likely to be faster by increasing frequencies of applied electric fields, while those works achieved larger reflection intensity change. With confocal microscopy, it was shown that the cores of the yolk−shell particles moved coherently parallel to the field under the application of an AC electric field, which decreased the scattering disorder of the core particles (Figure 8a). On the other hand, without an electric field, the cores exhibited random Brownian motion, which lowered the Bragg reflection peaks due to the increased disorder as expressed by the DW factor (Figure 8b).

Improved switchability of the Bragg peaks (i.e., an increased difference between the reflection peak intensities with and without applying an AC electric field) was achieved by increasing the particles' mobility range.[47] By increasing the electrolyte concentration of the surrounding medium and/or making the core size smaller, the motion range of cores increased so that the displacement disorder was increased as well (Figure 8c). Thus, the switchability of the reflection peak intensities was improved significantly by increasing the average squared distance of a core particle as characterized by the DW factor. The insights obtained in this study suggest that yolk−shell colloidal crystals are promising candidates for novel switchable photonic crystals of which photonic band gaps or structural colors can be controlled by AC electric fields with fast (≪1 s) response times.

■ ASSOCIATED CONTENT

Supporting Information

The Supporting Information is available free of charge at https://pubs.acs.org/doi/10.1021/acsaom.3c00392.

Synthesis details; calculated scattering cross-sectional area of a hollow silica shell and a S/T/S core; reflection spectra of a dried yolk−shell colloidal crystal and a hollow silica colloidal crystal; peak assignment in the reflection spectra; interaction potential calculation between two spheres in LiCl aqueous solution; zeta-potential measurement; scattering cross section of a S/T/S core plotted against the diameter; form factor of core particles; and statistics of the number of cores within a hollow shell (PDF)

Confocal core particles in a 2D array of a yolk−shell particles with the 100 Hz AC electric field on and off (electric field intensity being 25 V/mm and the scale bar 500 nm) (AVI)

Confocal 2D array of a yolk−shell particles in 85 v % DMSO aqueous solution with an external AC electric field on and off (electric field intensity being 25 V/mm and frequency 1.0 Hz) (AVI)

Yolk−shell colloidal crystals with an external AC electric field on and off (electric field intensity being 24 V_{pp}/mm and frequency 100 Hz) (AVI)

■ AUTHOR INFORMATION

Corresponding Authors

Kanako Watanabe − *Department of Chemical Engineering, Tohoku University, Sendai, Miyagi 980-8579, Japan;* orcid.org/0000-0003-2064-4391; Email: kanako.w@tohoku.ac.jp

Daisuke Nagao − *Department of Chemical Engineering, Tohoku University, Sendai, Miyagi 980-8579, Japan;* orcid.org/0000-0003-2710-5235; Email: dnagao@tohoku.ac.jp

Authors

Hikaru Namigata − *Department of Chemical Engineering, Tohoku University, Sendai, Miyagi 980-8579, Japan*

Tom A. J. Welling − *Department of Chemical Engineering, Tohoku University, Sendai, Miyagi 980-8579, Japan; Soft Condensed Matter, Debye Institute for Nanomaterials Science, Utrecht University, Utrecht 3584 CC, The Netherlands;* orcid.org/0000-0001-5958-4571

Keishi Suga − *Department of Chemical Engineering, Tohoku University, Sendai, Miyagi 980-8579, Japan;* orcid.org/0000-0001-8015-8729

Arnout Imhof − *Soft Condensed Matter, Debye Institute for Nanomaterials Science, Utrecht University, Utrecht 3584 CC, The Netherlands;* orcid.org/0000-0002-7445-1360

Alfons van Blaaderen − *Soft Condensed Matter, Debye Institute for Nanomaterials Science, Utrecht University, Utrecht 3584 CC, The Netherlands*

Complete contact information is available at: https://pubs.acs.org/10.1021/acsaom.3c00392

Author Contributions

H.N., K.W., and D.N. made contributions to conception and design of this study. H.N., T.W., and K.W. performed experiments and the data analysis. H.N. and K.W. prepared the original draft. T.W., K.S., A.I., A.B., and D.N. contributed to revise the manuscript. A.I., A.B., and D.N. supervised the study.

Funding

This research was supported by the Ministry of Education, Culture, Sports, Science and Technology (JSPS KAKENHI grant numbers 21K14491, 20K21097, 22H01843, and 22J11948) and Materials Processing Science project ("Materealize") of MEXT (grant number JPMXP0219192801).

Notes

The authors declare no competing financial interest.

■ ACKNOWLEDGMENTS

The authors thank technical support staff in the Department of Engineering, Tohoku University for electron microscopy images.

■ REFERENCES

(1) Armstrong, E.; O'Dwyer, C. Artificial Opal Photonic Crystals and Inverse Opal Structures - Fundamentals and Applications from Optics to Energy Storage. *J. Mater. Chem. C* **2015**, *3* (24), 6109−6143.

(2) Goldenberg, L. M.; Wagner, J.; Stumpe, J.; Paulke, B. R.; Görnitz, E. Ordered Arrays of Large Latex Particles Organised by Vertical Deposition. *Mater. Sci. Eng., C* **2002**, *22* (2), 405−408.

(3) Mine, E.; Hirose, M.; Kubo, M.; Kobayashi, Y.; Nagao, D.; Konno, M. Synthesis of Submicron-Sized Titania-Coated Silica Particles with a Sol-Gel Method and Their Application to Colloidal Photonic Crystals. *J. Sol-Gel Sci. Technol.* **2006**, *38* (1), 91−95.

(4) Liu, G.; Zhou, L.; Wu, Y.; Wang, C.; Fan, Q.; Shao, J. Optical Properties of Three-Dimensional P(St-MAA) Photonic Crystals on Polyester Fabrics. *Opt. Mater.* **2015**, *42*, 72−79.
(5) Lee, G. H.; Kim, J. B.; Choi, T. M.; Lee, J. M.; Kim, S. H. Structural Coloration with Nonclose-Packed Array of Bidisperse Colloidal Particles. *Small* **2019**, *15* (5), 1804548.
(6) Ueno, K.; Inaba, A.; Ueki, T.; Kondoh, M.; Watanabe, M. Thermosensitive, Soft Glassy and Structural Colored Colloidal Array in Ionic Liquid: Colloidal Glass to Gel Transition. *Langmuir* **2010**, *26* (23), 18031−18038.
(7) Lee, I.; Kim, D.; Kal, J.; Baek, H.; Kwak, D.; Go, D.; Kim, E.; Kang, C.; Chung, J.; Jang, Y.; Ji, S.; Joo, J.; Kang, Y. Quasi-Amorphous Colloidal Structures for Electrically Tunable Full-Color Photonic Pixels with Angle-Independency. *Adv. Mater.* **2010**, *22* (44), 4973−4977.
(8) Schertel, L.; Wimmer, I.; Besirske, P.; Aegerter, C. M.; Maret, G.; Polarz, S.; Aubry, G. J. Tunable High-Index Photonic Glasses. *Phys. Rev. Mater.* **2019**, *3* (1), 015203.
(9) Kim, H.; Ge, J.; Kim, J.; Choi, S. E.; Lee, H.; Lee, H.; Park, W.; Yin, Y.; Kwon, S. Structural Colour Printing Using a Magnetically Tunable and Lithographically Fixable Photonic Crystal. *Nat. Photonics* **2009**, *3* (9), 534−540.
(10) Lee, H. S.; Shim, T. S.; Hwang, H.; Yang, S.-M.; Kim, S.-H. Colloidal Photonic Crystals toward Structural Color Palettes for Security Materials. *Chem. Mater.* **2013**, *25* (13), 2684−2690.
(11) Kohri, M.; Tamai, Y.; Kawamura, A.; Jido, K.; Yamamoto, M.; Taniguchi, T.; Kishikawa, K.; Fujii, S.; Teramoto, N.; Ishii, H.; Nagao, D. Ellipsoidal Artificial Melanin Particles as Building Blocks for Biomimetic Structural Coloration. *Langmuir* **2019**, *35* (16), 5574−5580.
(12) Lan, N. X. V.; Moon, J.; Kang, T. H.; Wang, K.; Park, H. G.; Yi, G. R. Index-Matched Composite Colloidal Crystals of Core-Shell Particles for Strong Structural Colors and Optical Transparency. *Chem. Mater.* **2021**, *33* (5), 1714−1722.
(13) Yang, D.; Liao, G.; Huang, S. Hand Painting of Noniridescent Structural Multicolor through the Self-Assembly of YOHCO3 Colloids and Its Application for Anti-Counterfeiting. *Langmuir* **2019**, *35* (25), 8428−8435.
(14) Li, J.; Zheng, T. A Comparison of Chemical Sensors Based on the Different Ordered Inverse Opal Films. *Sens. Actuators, B* **2008**, *131* (1), 190−195.
(15) Holtz, J. H.; Asher, S. A. Polymerized Colloidal Crystal Hydrogel Films as Intelligent Chemical Sensing Materials. *Nature* **1997**, *389* (6653), 829−832.
(16) Dimitrov, A. S.; Nagayama, K. Continuous Convective Assembling of Fine Particles into Two-Dimensional Arrays on Solid Surfaces. *Langmuir* **1996**, *12* (5), 1303−1311.
(17) Qdemat, A.; Kentzinger, E.; Buitenhuis, J.; Rücker, U.; Ganeva, M.; Brückel, T. Self Assembled Monolayer of Silica Nanoparticles with Improved Order by Drop Casting. *RSC Adv.* **2020**, *10* (31), 18339−18347.
(18) Shieh, J.-Y.; Kuo, J.-Y.; Weng, H.-P.; Yu, H. H. Preparation and Evaluation of the Bioinspired PS/PDMS Photochromic Films by the Self-Assembly Dip-Drawing Method. *Langmuir* **2013**, *29* (2), 667−672.
(19) Kim, M. H.; Im, S. H.; Park, O. O. Rapid Fabrication of Two- and Three-Dimensional Colloidal Crystal Films via Confined Convective Assembly. *Adv. Funct. Mater.* **2005**, *15* (8), 1329−1335.
(20) Yahata, A.; Ishii, H.; Nakamura, K.; Watanabe, K.; Nagao, D. Three-Dimensional Periodic Structures of Gold Nanoclusters in the Interstices of Sub-100 Nm Polymer Particles toward Surface-Enhanced Raman Scattering. *Adv. Powder Technol.* **2019**, *30* (12), 2957−2963.
(21) Takeoka, Y. Stimuli-Responsive Opals: Colloidal Crystals and Colloidal Amorphous Arrays for Use in Functional Structurally Colored Materials. *J. Mater. Chem. C* **2013**, *1* (38), 6059−6074.
(22) Solomon, M. J. Tools and Functions of Reconfigurable Colloidal Assembly. *Langmuir* **2018**, *34* (38), 11205−11219.
(23) Li, C.; Zhou, X.; Wang, K.; Li, K.; Li, M.; Song, Y. Progress of Electrically Responsive Photonic Crystals. *Compos. Commun.* **2019**, *12*, 47−53.
(24) Puzzo, D. P.; Arsenault, A. C.; Manners, I.; Ozin, G. A. Electroactive Inverse Opal: A Single Material for All Colors. *Angew. Chem.* **2009**, *121* (5), 961−965.
(25) Comiskey, B.; Albert, J. D.; Yoshizawa, H.; Jacobson, J. An Electrophoretic Ink for All-Printed Reflective Electronic Displays. *Nature* **1998**, *394* (6690), 253−255.
(26) Fudouzi, H.; Xia, Y. Colloidal Crystals with Tunable Colors and Their Use as Photonic Papers. *Langmuir* **2003**, *19* (23), 9653−9660.
(27) Gallego-Gómez, F.; Morales, M.; Blanco, A.; López, C. Bare Silica Opals for Real-Time Humidity Sensing. *Adv. Mater. Technol.* **2019**, *4* (2), 1800493.
(28) He, J.; Shen, X.; Li, H.; Yao, Y.; Guo, J.; Wang, C. Scalable and Sensitive Humidity-Responsive Polymer Photonic Crystal Films for Anticounterfeiting Application. *ACS Appl. Mater. Interfaces* **2022**, *14*, 27251−27261.
(29) Honda, M.; Seki, T.; Takeoka, Y. Dual Tuning of the Photonic Band-Gap Structure in Soft Photonic Crystals. *Adv. Mater.* **2009**, *21* (18), 1801−1804.
(30) Sugiyama, H.; Sawada, T.; Yano, H.; Kanai, T. Linear Thermosensitivity of Gel-Immobilized Tunable Colloidal Photonic Crystals. *J. Mater. Chem. C* **2013**, *1* (38), 6103−6106.
(31) Kanai, T.; Kobayashi, N.; Tajima, H. Enhanced Linear Thermosensitivity of Gel-Immobilized Colloidal Photonic Crystal Film Bound on Glass Substrate. *Mater. Adv.* **2021**, *2* (8), 2600−2603.
(32) Tang, S.; Wang, C.; Liu, N.; Li, Y.; Han, P.; Lu, Q. Instantaneous Magnetically Assembled and Hydrophilic Photonic Crystals with Controlled Diffraction Colors. *J. Phys. Chem. C* **2018**, *122* (31), 18021−18028.
(33) Li, H.; Li, C.; Sun, W.; Wang, Y.; Hua, W.; Liu, J.; Zhang, S.; Chen, Z.; Wang, S.; Wu, Z.; Zhu, Q.; Tang, R.; Yu, J.; He, L.; Ozin, G. A.; Zhang, X. Single-Stimulus-Induced Modulation of Multiple Optical Properties. *Adv. Mater.* **2019**, *31* (23), 1900388.
(34) Chen, K.; Fu, Q.; Ye, S.; Ge, J. Multicolor Printing Using Electric-Field-Responsive and Photocurable Photonic Crystals. *Adv. Funct. Mater.* **2017**, *27* (43), 1702825.
(35) Fu, Q.; Zhu, H.; Ge, J. Electrically Tunable Liquid Photonic Crystals with Large Dielectric Contrast and Highly Saturated Structural Colors. *Adv. Funct. Mater.* **2018**, *28* (43), 1804628.
(36) Iwata, N.; Koike, T.; Tokuhiro, K.; Sato, R.; Furumi, S. Colloidal Photonic Crystals of Reusable Hydrogel Microparticles for Sensor and Laser Applications. *ACS Appl. Mater. Interfaces* **2021**, *13* (48), 57893−57907.
(37) Shah, A. A.; Ganesan, M.; Jocz, J.; Solomon, M. J. Direct Current Electric Field Assembly of Colloidal Crystals Displaying Reversible Structural Color. *ACS Nano* **2014**, *8* (8), 8095−8103.
(38) Kamata, K.; Lu, Y.; Xia, Y. Synthesis and Characterization of Monodispersed Core-Shell Spherical Colloids with Movable Cores. *J. Am. Chem. Soc.* **2003**, *125* (9), 2384−2385.
(39) Lou, X. W.; Archer, L. A.; Yang, Z. Hollow Micro-/Nanostructures: Synthesis and Applications. *Adv. Mater.* **2008**, *20*, 3987−4019.
(40) Priebe, M.; Fromm, K. M. Nanorattles or Yolk-Shell Nanoparticles-What Are They, How Are They Made, and What Are They Good For? *Chem.—Eur. J.* **2015**, *21* (10), 3854−3874.
(41) Okada, A.; Nagao, D.; Ueno, T.; Ishii, H.; Konno, M. Colloidal Polarization of Yolk/Shell Particles by Reconfiguration of Inner Cores Responsive to an External Magnetic Field. *Langmuir* **2013**, *29* (28), 9004−9009.
(42) Ruhl, T.; Spahn, P.; Hermann, C.; Jamois, C.; Hess, O. Double-Inverse-Opal Photonic Crystals: The Route to Photonic Bandgap Switching. *Adv. Funct. Mater.* **2006**, *16* (7), 885−890.
(43) Camargo, P. H. C.; Li, Z.-Y.; Xia, Y. Colloidal Building Blocks with Potential for Magnetically Configurable Photonic Crystals. *Soft Matter* **2007**, *3* (10), 1215.

https://doi.org/10.1021/acsaom.3c00392
ACS Appl. Opt. Mater. 2024, 2, 181−190

(44) Morozov, K. I.; Leshansky, A. M. Photonics of Template-Mediated Lattices of Colloidal Clusters. *Langmuir* **2019**, *35* (11), 3987−3991.
(45) Watanabe, K.; Ishii, H.; Konno, M.; Imhof, A.; van Blaaderen, A.; Nagao, D. Yolk/Shell Colloidal Crystals Incorporating Movable Cores with Their Motion Controlled by an External Electric Field. *Langmuir* **2017**, *33* (1), 296−302.
(46) Welling, T. A. J.; Grau-Carbonell, A.; Watanabe, K.; Nagao, D.; de Graaf, J.; van Huis, M. A.; van Blaaderen, A. Frequency-Controlled Electrophoretic Mobility of a Particle within a Porous, Hollow Shell. *J. Colloid Interface Sci.* **2022**, *627*, 761−773.
(47) Welling, T. A. J.; Watanabe, K.; Grau-Carbonell, A.; de Graaf, J.; Nagao, D.; Imhof, A.; van Huis, M. A.; van Blaaderen, A. Tunability of Interactions between the Core and Shell in Rattle-Type Particles Studied with Liquid-Cell Electron Microscopy. *ACS Nano* **2021**, *15* (7), 11137−11149.
(48) Graf, C.; Vossen, D. L. J.; Imhof, A.; van Blaaderen, A. A General Method to Coat Colloidal Particles with Silica. *Langmuir* **2003**, *19* (17), 6693−6700.
(49) Zhang, L.; D'Acunzi, M.; Kappl, M.; Auernhammer, G. K.; Vollmer, D.; van Kats, C. M.; van Blaaderen, A. Hollow Silica Spheres: Synthesis and Mechanical Properties. *Langmuir* **2009**, *25* (5), 2711−2717.
(50) Namigata, H.; Watanabe, K.; Okubo, S.; Nagao, D. Polymer-Coating of Photocatalytic Particles to Prevent Sintering in Their Calcination Process. *Colloids Surf., A* **2020**, *599*, 124782.
(51) Namigata, H.; Watanabe, K.; Okubo, S.; Hasegawa, M.; Suga, K.; Nagao, D. Double-Inverse-Opal-Structured Particle Assembly as a Novel Immobilized Photocatalytic Material. *Materials* **2020**, *14* (1), 28.
(52) He, S.; Zhang, W.; Liu, L.; Huang, Y.; He, J.; Xie, W.; Wu, P.; Du, C. Baseline Correction for Raman Spectra Using an Improved Asymmetric Least Squares Method. *Anal. Methods* **2014**, *6* (12), 4402−4407.
(53) Baek, S.-J.; Park, A.; Ahn, Y.-J.; Choo, J. Baseline Correction Using Asymmetrically Reweighted Penalized Least Squares Smoothing. *Analyst* **2015**, *140* (1), 250−257.
(54) LeBel, R. G.; Goring, D. A. I. Density, Viscosity, Refractive Index, and Hygroscopicity of Mixtures of Water and Dimethyl Sulfoxide. *J. Chem. Eng. Data* **1962**, *7* (1), 100−101.
(55) Takeoka, Y.; Watanabe, M. Template Synthesis and Optical Properties of Chameleonic Poly(N-Isopropylacrylamide) Gels Using Closest-Packed Self-Assembled Colloidal Silica Crystals. *Adv. Mater.* **2003**, *15* (3), 199−201.
(56) Míguez, H.; Meseguer, F.; López, C.; Mifsud, A.; Moya, J. S.; Vázquez, L. Evidence of FCC Crystallization of SiO2 Nanospheres. *Langmuir* **1997**, *13* (23), 6009−6011.
(57) Kobayashi, Y.; Miyauchi, H.; Gu, S.; Nagao, D.; Konno, M. Fabrication of Mono- and Multi-Layers of Submicron-Sized Spheres by a Dip-Coating Technique and Their Transmittance Property. *J. Chem. Eng. Jpn.* **2004**, *37* (5), 614−621.
(58) Wang, J.; Sugawara-Narutaki, A.; Fukao, M.; Yokoi, T.; Shimojima, A.; Okubo, T. Two-Phase Synthesis of Monodisperse Silica Nanospheres with Amines or Ammonia Catalyst and Their Controlled Self-Assembly. *ACS Appl. Mater. Interfaces* **2011**, *3* (5), 1538−1544.
(59) Mikhnev, L. V.; Bondarenko, E. A.; Chapura, O. M.; Skomorokhov, A. A.; Kravtsov, A. A. Influence of Annealing Temperature on Optical Properties of the Photonic-Crystal Structures Obtained by Self-Organization of Colloidal Microspheres of Polystyrene and Silica. *Opt. Mater.* **2018**, *75*, 453−458.
(60) Shinohara, T.; Sogami, I. S.; Tanigawa, M.; Yoshiyama, T.; Yamada, H.; Oka, H.; Ise, N. Gravitational Sedimentation Effect of Colloidal Silica Crystals in Binary Systems of Titanium Dioxide and Silica Particles. *Phase Transitions* **2007**, *80* (8), 875−886.
(61) McRae, R.; Haymet, A. D. J. Freezing of Polydisperse Hard Spheres. *J. Chem. Phys.* **1988**, *88* (2), 1114−1125.
(62) Bolhuis, P. G.; Kofke, D. A. Monte Carlo Study of Freezing of Polydisperse Hard Spheres. *Phys. Rev. E: Stat., Nonlinear, Soft Matter Phys.* **1996**, *54* (1), 634−643.
(63) Pusey, P. N.; Zaccarelli, E.; Valeriani, C.; Sanz, E.; Poon, W. C. K. K.; Cates, M. E. Hard Spheres: Crystallization and Glass Formation. *Philos. Trans. R. Soc., A* **2009**, *367* (1909), 4993−5011.
(64) Pusey, P. N.; van Megen, W. Phase Behaviour of Concentrated Suspensions of Nearly Hard Colloidal Spheres. *Nature* **1986**, *320* (6060), 340−342.
(65) Davis, K. E.; Russel, W. B.; Glantschnig, W. J. Disorder-to-Order Transition in Settling Suspensions of Colloidal Silica: X-Ray Measurements. *Science* **1989**, *245* (4917), 507−510.
(66) Yethiraj, A.; van Blaaderen, A. A Colloidal Model System with an Interaction Tunable from Hard Sphere to Soft and Dipolar. *Nature* **2003**, *421* (6922), 513−517.
(67) Rodríguez-González, B.; Salgueiriño-Maceira, V.; García-Santamaría, F.; Liz-Marzán, L. M. Fully Accessible Gold Nanoparticles within Ordered Macroporous Solids. *Nano Lett.* **2002**, *2* (5), 471−473.
(68) Welling, T. A. J.; Kurioka, K.; Namigata, H.; Suga, K.; Nagao, D.; Watanabe, K. Highly Reflective and Transparent Shell-Index-Matched Colloidal Crystals of Core-Shell Particles for Stacked RGB Films. *ACS Appl. Nano Mater.* **2023**.
(69) Bierbaum, A.; Dux, C.; Versmold, H. Observation of the Debye-Waller Factor in a Colloidal Single Crystal. *Mol. Phys.* **1998**, *93* (4), 615−618.
(70) Jin, Z. H.; Gumbsch, P.; Lu, K.; Ma, E. Melting Mechanisms at the Limit of Superheating. *Phys. Rev. Lett.* **2001**, *87* (5), 055703.
(71) Van Hoang, V.; Phuoc Duy, T. Melting of Mesoscale Lennard-Jones Crystals with Free Surfaces. *J. Phys. Soc. Jpn.* **2013**, *82* (6), 064601.
(72) van der Meer, B.; Qi, W.; Fokkink, R. G.; van der Gucht, J.; Dijkstra, M.; Sprakel, J. Highly Cooperative Stress Relaxation in Two-Dimensional Soft Colloidal Crystals. *Proc. Natl. Acad. Sci. U.S.A.* **2014**, *111* (43), 15356−15361.
(73) Yu, S.; Cao, X.; Niu, W.; Wu, S.; Ma, W.; Zhang, S. Large-Area and Water Rewriteable Photonic Crystal Films Obtained by the Thermal Assisted Air-Liquid Interface Self Assembly. *ACS Appl. Mater. Interfaces* **2019**, *11*, 22777−22785.
(74) Zhou, C.; Qi, Y.; Zhang, S.; Niu, W.; Wu, S.; Ma, W.; Tang, B. Water Rewriteable Double-Inverse Opal Photonic Crystal Films with Ultrafast Response Time and Robust Writing Capability. *Chem. Eng. J.* **2022**, *439*, 135761.

https://doi.org/10.1021/acsaom.3c00392
ACS Appl. Opt. Mater. 2024, 2, 181−190